

**PAPER**

State-dependent misalignment and turbulence effects on high-dimensional quantum key distribution with orbital angular momentum

OPEN ACCESS**RECEIVED**
30 January 2024**REVISED**
1 May 2024**ACCEPTED FOR PUBLICATION**
10 May 2024**PUBLISHED**
23 May 2024

Original Content from
this work may be used
under the terms of the
[Creative Commons
Attribution 4.0 licence](#).

Any further distribution
of this work must
maintain attribution to
the author(s) and the title
of the work, journal
citation and DOI.

Jiahao Li^{1,2,3}, Xingyu Wang^{1,3} , Huicun Yu¹, Jie Tang¹, Ying Liu¹, Yuexiang Cao¹ , Zhifeng Deng¹,
Dan Wu¹, Haoran Hu¹, Ya Wang¹, Huazhi Lun¹, Bo Zhang¹, Jiahua Wei¹, Bo Liu² and Lei Shi^{1,*}¹ School of Information and Navigation, Air Force Engineering University, Xi'an 710077, People's Republic of China² College of Advanced Interdisciplinary Studies, National University of Defense Technology, Changsha 410073, People's Republic of China³ These authors contributed equally to this work.

* Author to whom any correspondence should be addressed.

E-mail: slfly2012@163.com**Keywords:** quantum key distribution, orbital angular momentum, atmospheric channel model, security analysis**Abstract**

High-dimensional quantum key distribution (HD-QKD) is a topic of growing interest in the quantum communication community, not only for its inherent properties but also for its possible applications. As the typical freedom in HD-QKD, orbital angular momentum (OAM) has made significant advancements in experiments recently. However, in the airborne scenario, different states suffer different amounts of misalignment and turbulence. A complete theoretical analysis model for the transmission characteristics of OAM in atmospheric channels is lacking. In this paper, we systematically analyze the extent to which degeneration including channel power loss and mode crosstalk are influenced by misalignment and turbulence effects. Furthermore, the performance of OAM-encoded HD-QKD system in different dimensions is evaluated while incorporating finite-key effects. We demonstrate that the performance of OAM-encoded HD-QKD will be better at short range, which provide a reference to implement QKD based on task requirements. Since OAM is desired to increase the capacity of QKD system and experiments have already been carried out, our work can not only bridge the gap between theory and practice, but also optimize experimental parameters and improve system performance.

1. Introduction

Quantum key distribution (QKD), as a potentially revolutionary cryptographic technique, can establish a bit string of common true random bits between two legitimate parties. Based on quantum mechanics, QKD could provide information-theoretic approach against an eavesdropper during key distribution tasks [1–3]. Currently, along with the breakthrough of fiber-based [4–6] and satellite-based [7, 8] quantum communication, building and operating a high-efficient and flexible quantum internet has become a grand vision attracting global attention [9, 10]. However, most of these achievements are based on encoding information with two-dimensional quantum systems such as polarization and phase of photons. Although these systems are advantageous in qubit manipulation and control, the information capacity is limited to 1 bit per photon due to the intrinsically bounded Hilbert space. To break through the system information entropy threshold, high-dimensional (HD) QKD offers an exceptional means and has developed rapidly in both theoretical [11–15] and experimental [16–20] aspects over past two decades. By utilizing larger Hilbert space, HD-QKD has following benefits [21]:

- (1) Information and communication capacity;
- (2) Higher noise resilience;
- (3) Enhanced robustness to quantum cloning;

- (4) Larger violation of local theories;
- (5) Advantages in communication complexity problems.

Although significant progress has been made in generating and manipulating HD quantum states, reliable transmission still remains an open challenge for construction of future quantum networks. At present, HD quantum systems have been demonstrated using various degrees of freedom of the photon, such as time-bin encoding [22–24] or spatial modes [16, 19, 25]. Time-bin encoding has the ability of preserving states during propagation, and is compatible with existing networks [26–28]. Orbital angular momentum (OAM) is one of the most frequently exploited spatial modes to realize HD quantum systems [29, 30]. The OAM states of quantum number span an arbitrarily large Hilbert space, which provide an infinite number of available eigenstates for QKD systems in principle [31]. Due to high crosstalk between the optical modes between the propagation in standard multimode fiber, special fibers like air-core fiber [32], multicore fiber [33] and vortex fiber [34] are selected to transmit OAM. Because the OAM mode is difficult to match the eigenmode of fiber, OAM transmission is mainly applied to free-space channel [35].

According to the transmission characteristics of OAM in atmospheric turbulence, combined with airborne scenario can be used as a supplement to the integrated quantum communication network. Different from the fixed motion trajectory of satellite scenario more suitable to time-bin encoding [36], the performance of airborne scenario is restricted by the high-speed maneuvering of the airborne platform and the misalignment of the polarization reference frame caused by random attitude. By using the rotational invariance of OAM beam [37], the problem of ground-to-air scene alignment can be effectively avoided, and a new coding scheme is provided for the construction of high-speed and stable mobile quantum communication networks for airborne platforms. Nevertheless, the helical phase of a vortex beam that carries OAM is sensitive to the turbulent channel and easily distorted, which directly leads to both optical communication and quantum cryptography system performance deterioration [38–42]. There are some critical issues in an OAM-encoded QKD system under airborne scenario, including channel power loss, mode crosstalk, etc. Specifically, the challenges from the channel transmission come from divergency, misalignment and turbulence.

The geometric attenuation caused by OAM beam divergence is the main factor affecting the transmission efficiency [43]. However, vortex beam with different OAM index ℓ exists state-dependent diffraction (SDD) [44–47], leading to an increased error rate and security loophole at receiver. Misalignment is an important factor that determines the performance and stability of free-space optical communication system. In an airborne link, the receiver should be able to distinguish the OAM modes. Due to the vibrations and jitter from transceivers and atmospheric turbulence, the pointing error caused by misalignment will result in mode crosstalk of OAM and reduce the mode purity [48–50]. Local refractive index fluctuations at any position in atmospheric turbulence introduce a random phase distortion to the transverse beam profile of OAM beams. Such phase distortion induces dynamic modal coupling and channel crosstalk, and further contribute to decrease of the quantum state fidelity [51–53]. To address these challenges, a large amount of research focuses on compensation of system performance. The main methods include: new protocol of communication coding [54, 55], adaptive optics [56–59], and correction of wavefront aberration with machine learning methods [60, 61]. However, there is lack of detailed analysis for the practical security of OAM-encoded QKD in theory.

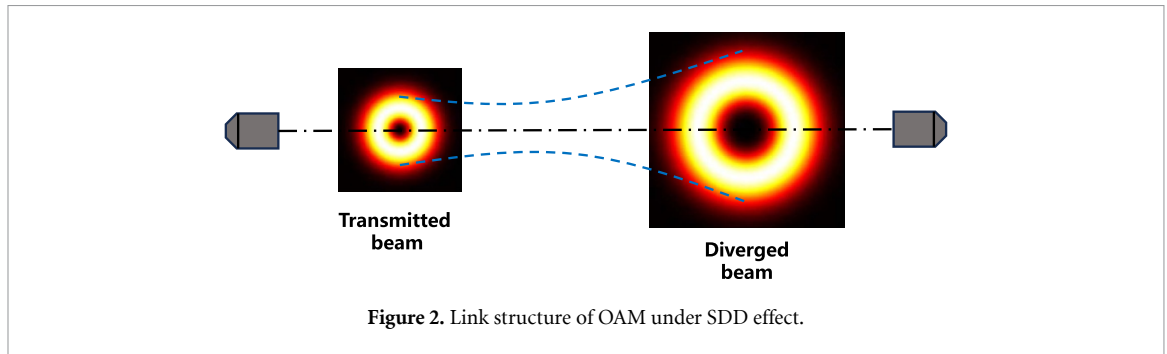
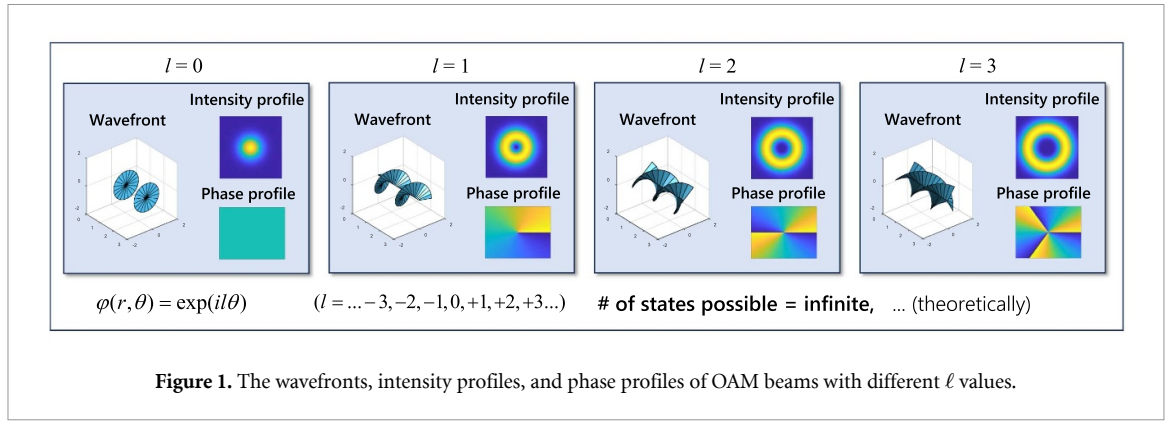
To close the gap between theory and practice, in this paper, we establish a complete OAM atmospheric transmission model in airborne scenario, with emphasis on state-dependent misalignment and turbulence effects. Incorporating finite-key effects, a security analysis of OAM-encoded HD-QKD is conducted to allow for the quantitative assessment of secure key rate (SKR) and quantum bit error rate (QBER). Our analysis are further able to provide theoretical support for optimizing experimental parameters and improving system performance.

2. Challenges in an OAM-based channel

Based on the advantages of high-dimensional coding, OAM modes could be potentially utilized in free space optical (FSO) communication. However, for complex atmospheric environment, there are different key challenges, which might induce power loss and mode crosstalk. Several critical factors cannot be ignored including atmospheric turbulence, divergency and misalignment. Some details about potential challenges will be discussed in this section. The concept of OAM beam is introduced firstly.

2.1. OAM of light beam

Due to the phase singularity in a helical phase profile, an OAM beam with a nonzero order usually has a donut-shaped intensity profile, as shown in figure 1. In general, an OAM beam could refer to any helically



phased light beam, irrespective of its radial distribution. Laguerre–Gaussian (LG) modes are exploited as the orthogonal modal basis set of OAMs. The complex amplitude expression of OAM beam in LG mode is:

$$\varphi_{l,p}(r, \theta, z) = \frac{A}{w(z)} \left(\frac{\sqrt{2}r}{w(z)} \right)^{|l|} L_p^{|l|} \left(\frac{2r^2}{w^2(z)} \right) \times \exp\left(-\frac{r^2}{w^2(z)} \right) \exp(il\theta) \quad (1)$$

where normalizing factor $A = \sqrt{2p!/\pi(|l|+p)!}$, the indices l and p correspond to azimuthal and radial distribution, respectively. $w(z) = w_0 \sqrt{1 + z^2/z_R^2}$ represents the spot size of the LG beam transmitted to the distance z . w_0 is the beam waist, $z_R = \frac{1}{2}kw_0^2$ is the Rayleigh range, $k = 2\pi/\lambda$ and λ is wavelength. $L_p^{|l|}(\cdot)$ are the generalized Laguerre polynomials and (r, θ, z) is the cylindrical coordinate.

The intensity distribution of a LG mode for the lowest-order radial mode ($p = 0$) is:

$$I_l(r, \theta, z) = |A_{l,p}(r, \theta, z)|^2 = \frac{2}{w^2(z)\pi|l|!} \left(\frac{\sqrt{2}r}{w(z)} \right)^{2|l|} \times \exp\left(-\frac{2r^2}{w^2(z)} \right) \quad (2)$$

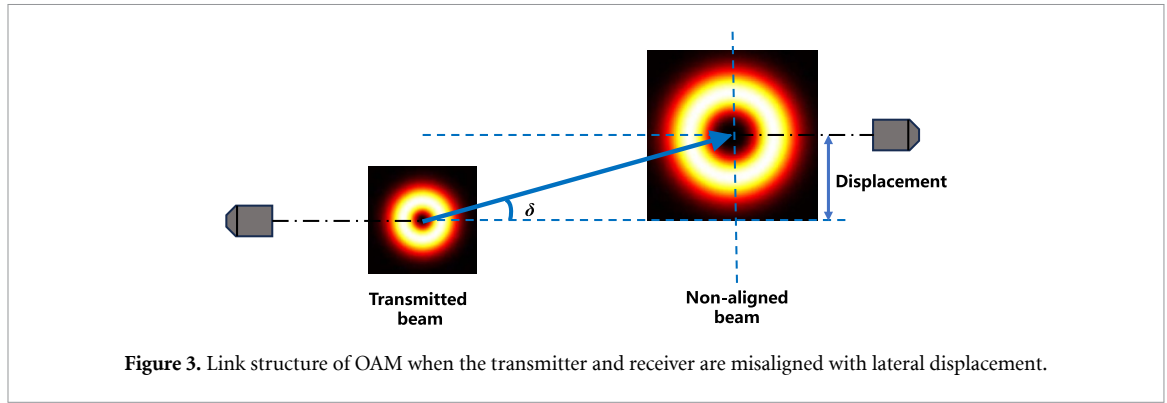
where $A_{l,p}(r, \theta, z)$ represents the amplitude of the OAM beam. For ease of calculation, the expression is normalized such that $\iint I_l(r, \theta, z) r dr d\theta = 1$.

2.2. State-dependent divergence

Limited by the size of optical components like limited-size receiver aperture, the transmission of OAM beam in free space is affected by SDD. In such a scenario, different states (azimuthal mode) ℓ experience different amounts of diffraction, leading to state-dependent loss. The reason is that the mode transmission efficiency induced by SDD is a function of Fresnel product N_f and OAM quantum number ℓ . According to the research of [44], the radial position of the maximum of intensity is:

$$r(I_{\max}) = \sqrt{\frac{|l|}{2}} w(z) \quad (3)$$

which confirms the existence of SDD. Link structure of OAM under SDD effect is shown in the figure 2.



The beam divergence could increase the difficulty of capturing the beam profiles, which contributes to signal power loss. Since the distribution of light intensity is normalized, the geometric attenuation L_{geo} caused by diffraction could be obtained by calculating the optical power at the receiving end:

$$\begin{aligned} L_{\text{geo}} &= \frac{P_R}{P_T} = \int_A I_l(r, \theta, z) = \int_0^{D_r/2} I_l(r, \theta, z) \times 2\pi r dr \\ &= -\Gamma\left(|l| + 1, \frac{2r^2}{w^2(z)}\right) \Big|_0^{D_r/2} \end{aligned} \quad (4)$$

where, A represents the aperture area of the receiving telescope, $\Gamma(s, t)$ represents an incomplete gamma function.

Because of the SDD, OAM states with higher ℓ will have larger far-field sizes, and acquire more propagation phase. Thus, in practical free-space communication links, different OAM states will suffer different amounts of loss for a given collection aperture of finite size, leading to ℓ -dependent detection efficiency.

2.3. State-dependent misalignment

In FSO links, mechanical errors in the acquiring, pointing and tracking (APT) system and vibrations of the transmitter/receiver platform will cause the random beam jitters, contributing to the fluctuating losses. Assuming a Gaussian beam, the misalignment could lead to power loss, as the limited-size receiver aperture might fail to fully capture the beam profile. However, in an OAM-based communication link, such misalignment could induce not only power loss but also inter-channel crosstalk, which would affect the SKR and QBER.

Due to the special beam profile of OAM, lateral displacement is analyzed emphatically to ensure the receiving efficiency. Figure 3 shows the link structure of OAM when the transmitter and receiver are misaligned with lateral displacement.

In scenario of lateral displacement, based on central limit theorem, the random position deviations and caused by jitter can be assumed to be Gaussian random variables with a mean of zero and a variance σ_ρ^2 . Jitter variance σ_ρ^2 represents stability of the transmitter. ρ denotes the radial vector representing random beam displacements. Due to the symmetry of the beam shape and receiver area, the characterization of transmittance efficiency caused by misalignment η_{pe} depends only on the radial jitter distance $\rho = \|\rho\|$. So ρ can be described by the Rayleigh distribution:

$$f_\rho(\rho) = \frac{\rho}{\sigma_\rho^2} \times \exp\left(-\frac{\rho^2}{2\sigma_\rho^2}\right), \rho > 0. \quad (5)$$

Given the factor of misalignment, the expression (2) of intensity distribution could be calculated renewedly:

$$I_l(r - \rho, \theta, z) = \frac{2}{w^2(z) \pi |l|!} \left(\frac{\sqrt{2}(r - \rho)}{w(z)}\right)^{2|l|} \times \exp\left(-\frac{2(r - \rho)^2}{w^2(z)}\right). \quad (6)$$

Under the limited receiving aperture effect, transmittance efficiency caused by lateral displacement can be expressed:

$$L_{pe}(\rho) = \frac{P_R}{P_T} = \int_A I_l(r - \rho, \theta, z). \quad (7)$$

In the case of misalignment, the power of OAM beams received on each circle of the receiving telescope varies, so the method of calculating the received optical power by using polar coordinates is no longer applicable. Here, the point coordinate method is applied to obtain the surface integral.

$$L_{pe}(\rho) = L_{pe}(\Delta x, \Delta y) = \int_A I_l(x + \Delta x, y + \Delta y, z) dx dy \quad (8)$$

where $(\Delta x)^2 + (\Delta y)^2 = \rho^2$. Replace the telescope area A with a square aperture of area $\pi(D_R/2)^2$.

$$L_{pe}(\rho) \approx \int_{-\xi}^{\xi} \int_{-\xi}^{\xi} \frac{2}{w^2(z) \pi |l|!} \left\{ \frac{2[(x-\rho)^2 + y^2]}{w^2(z)} \right\}^{|l|} \times \exp \left\{ -\frac{2[(x-\rho)^2 + y^2]}{w^2(z)} \right\} dx dy \quad (9)$$

where $\xi = \sqrt{\pi} D_r/2$. Because ρ obeys the Rayleigh distribution, received power (also called transmittance efficiency) caused by misalignment is given as:

$$\eta_{pe} = \int_0^{\infty} L_{pe}(\rho) f_{\rho}(\rho) d\rho. \quad (10)$$

In order to get closer to the practical application, we analyze the displacement errors at different distances. The geometric variance of the pointing error at the receiver can be approximated by [62]:

$$\sigma_{\rho}^2(z) = \pi \tan^2(\delta/2) z^2 \quad (11)$$

where δ is the angular jitter error at the transmitter. For small amounts of δ one can write $\sigma_{\rho}^2(z) \simeq (\delta z)^2$.

Furthermore, misalignment will also cause bit error, that is, lateral displacement will lead to energy transfer between receiving OAM beam modes. The mode purity of an OAM state will decrease accordingly, which contributes to incorrect receiving bits. Assuming the radial and angular deviation of OAM beam under the action of misalignment is ρ and α , respectively. The complex amplitude expression of deflected l -state OAM beam could be expanded in form of spiral harmonic function:

$$\varphi(r, \theta, z) = \frac{1}{\sqrt{2\pi}} \sum_{m=-\infty}^{\infty} A_{ml}(r, \rho) \times \exp[im\theta - i(m-l)\alpha] \quad (12)$$

where $A_{ml}(r, \rho) = \frac{E_l}{w(z)^l} \exp(-\frac{r^2 + \rho^2}{w(z)^2}) \sum_{n=0}^l C_l^n r^n (-\rho)^{l-n} J_{m-n}(\frac{2r\rho}{w(z)^2})$ represents amplitude component of m -state OAM beam. E_l is amplitude, and $J_m(x)$ is the modified Bessel function of the first kind of integer m .

According to the formula (12), the orientation error causes mode expansion of pure l -state OAM beam, and the power spectrum of the mode is symmetrically distributed with order $m = l$ as the center. Therefore, when the OAM beam is transmitted along different axes, it is the result of the superposition of different OAM modes on the measurement axis. Below, we represent the proportion distribution of different modes according to the energy weight distribution. The energy of the received beam can be expressed as:

$$U = 2\varepsilon_0 \sum_{m=-\infty}^{\infty} C_m \quad (13)$$

where $C_m = \int_0^{D_r/2} |A_{ml}(r, \rho)|^2 r dr$ represents the probability density of OAM beams revealing in m -state. ε_0 is permittivity of vacuum.

The weight factor of each harmonic component represents the ratio of the energy of each spiral harmonic with different OAM states to the total energy of the beam. Therefore, influenced by pointing error, the probability of received correct OAM state can be given as:

$$P_{pe} = \frac{C_m}{\sum_{q=-\infty}^{\infty} C_q}. \quad (14)$$

According to formulas (9) and (12), both the detection efficiency and probability caused by misalignment are related to OAM index l , which theoretically proves the existence of state-dependent misalignment.

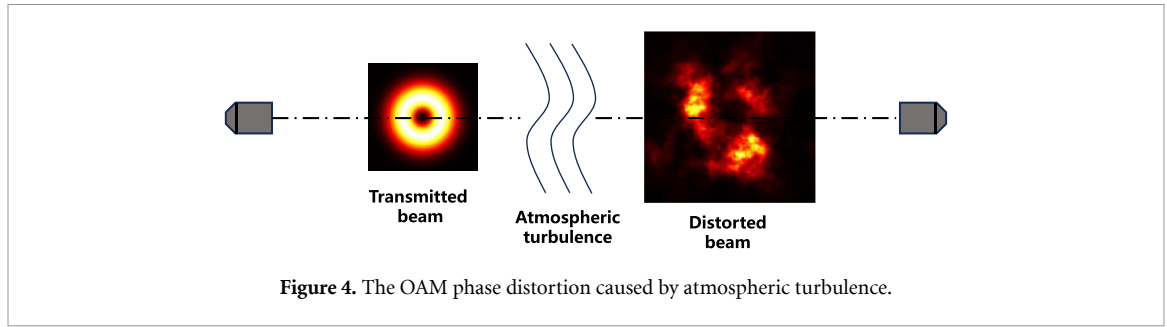


Figure 4. The OAM phase distortion caused by atmospheric turbulence.

2.4. State-dependent turbulence

Atmospheric turbulence refers to irregular motion in the atmosphere. Specifically, temperature fluctuations and air currents in a turbulent atmosphere cause the appearance of eddies. These eddies lead to fluctuations of the local index of refraction at any position in the atmosphere. This deterioration becomes particularly evident in OAM communication. The reason lies in the phase distortion caused by atmospheric turbulence. The phase distortion will cause the wavefront distortion of OAM beams, so that the peak position of OAM beams will be shifted and the information transmission will be interfered. The phase distortion caused by atmospheric turbulence is shown in figure 4.

During practical implementation, a beacon light can be used to eliminate the low order aberrations from turbulence. Therefore, this scenario focuses on wavefront distortion caused by state-dependent turbulence. From literature [51], the Kolmogorov turbulence theory is used to evaluate the random statistics of atmospheric turbulence. The probability that OAM beam with quantum number l receives OAM beam with quantum number m after transmission is:

$$\langle s_{\Delta} \rangle = \frac{1}{\pi} \int_0^1 \int_0^{2\pi} \exp\left(-3.44 \left(\frac{D_r y \sin(\theta/2)}{r_0}\right)^{5/3}\right) \cos \Delta \theta y d\theta dy \quad (15)$$

where $r_0 = 0.1853 \left(\frac{\lambda^2}{C_n^2 z}\right)^{3/5}$ represents Fried parameter, C_n^2 is the refractive-index structure parameter, which is the strength of atmosphere turbulence. λ is the wavelength. $\Delta = |l - m|$.

The transmission probability η_{atm} , which illustrates the probability of the received photon with the same OAM state as the input, is used to describe the aberration about atmospheric turbulence and link attenuation. η_{atm} is expressed as:

$$\eta_{\text{atm}} = \langle s_0 \rangle \exp(-\beta z) \quad (16)$$

where $\langle s_0 \rangle$ represents the mode purity of the receiving initial OAM state. Without loss of generality, we are only interested in the ensemble average of this quantity. β is the link attenuation coefficient. Correspondingly, the transmission error probability is $\eta_{\text{atm}} = 1 - \eta_{\text{atm}}$.

It is similar to the analysis of the pointing error on the receiving probability of the helical spectrum. The same formula $C_l = \int_0^{D_r/2} |a_l(r, z)|^2 r dr$ applies to atmospheric turbulence.

According to the analysis in section 2.3, it can be concluded that in atmospheric turbulence, the helical harmonic C_l with OAM index l is:

$$C_l = \frac{2\pi A^2}{w^2(z)} \int_0^{D_r/2} \left(\frac{\sqrt{2}r}{w(z)}\right)^{2|m|} \left[L_p^{|m|}\left(\frac{2r^2}{w^2(z)}\right)\right]^2 \times \exp\left(\frac{-2r^2}{w^2(z)} - \frac{2r^2}{r_0^2}\right) \times I_{l-m}\left(\frac{2r^2}{r_0^2}\right) r dr. \quad (17)$$

It is worth mentioning that the above analysis of state-dependent turbulence includes two folds: (1) high order OAMs have larger beam cross section which leads to a worse turbulence; (2) high order OAMs have multi-fold phase structures which are more sensitive to phase distortions. Therefore, influenced by atmospheric turbulence, the probability of received correct OAM state can be given as:

$$P_{\text{at}} = \frac{C_{l_0}}{\sum_{l=-\infty}^{\infty} C_l}. \quad (18)$$

Formula (18) represents the normalized energy weight for each of the spiral harmonics of OAM beams in the paraxial region. Formulas (15) and (17) show that the influence of OAM in turbulence is also related to state.

3. Influence on decoy-state OAM-encoded HD-QKD

3.1. Analysis on the key generation rate performance

In OAM-encoded HD-QKD, the SUP basis and the OAM basis form two mutually unbiased bases, which guarantees the unconditional security of QKD. OAM basis is composed of different OAM states, and the Fourier conjugate SUP basis consists of an equal superposition of OAM states with fixed relative phase between adjacent OAM components. The OAM basis and SUP basis can be represented as:

$$\begin{aligned} \{|\varphi_{\text{OAM}}\rangle\} &= \{|-L\rangle, |-L+1\rangle, \dots, |0\rangle, \dots, |L-1\rangle, |L\rangle\} \\ \{|\psi_{\text{SUP}}\rangle\} &= \left\{ \frac{1}{\sqrt{d}} \sum_{l=-L}^L \exp\left(i\frac{j2\pi}{d}\right) |\varphi_{\text{OAM}}\rangle \right\} \end{aligned} \quad (19)$$

where d is the dimension of the Hilbert space and L is the maximum OAM quantum number in use, which satisfies the relation $2L + 1 = d$.

Generally, Alice independently modulates quantum states by spatial light modulator. Then, the weak coherent pulses are attenuated to the single-photon level. Another attenuator is used to realize the ‘vacuum + weak decoy state’ method [63]. The OAM beams are transmitted in free-space link. In measurement parts, photons carrying OAM are detected by OAM sorters and single-photon detector (SPD). Bob applies two different mode sorters to fully discriminate quantum states in a specific dimension, one is used to measure the OAM basis, the other constructs the regulation required by the mapping to obtain the SUP basis according to the mathematical transformation method. Subsequently, Bob uses the results with OAM basis as the key bits and the results with SUP basis as the testing bits, and then testify the security of the key distribution. After post-processing procedure containing basis sifting, error estimation, key reconciliation, error verification, and privacy amplification, QKD implements secure key distribution.

The deterioration on OAM-encoded HD-QKD in free space from divergence, misalignment and turbulence concentrate on SKR and QBER. According to the Gottesman–Lo–Lütkenhaus–Preskill formula [64] for HD-QKD, the secret key rate of the d -dimensional BB84-QKD can be estimated by:

$$R \geq q_m Q_\mu^{\text{OAM}} \left\{ -f_{\text{EC}}(E_\mu^{\text{OAM}}) H_d(E_\mu^{\text{OAM}}) + \Delta_1 [\log_2 d - H_d(e_1^{\text{SUP}})] \right\} \quad (20)$$

where q_m represents the probability of choosing basis and depends on the QKD protocol. Q_μ^{OAM} and E_μ^{OAM} are the gain and QBER of the signal states, respectively. Δ_1 is the fraction of single-photon signals transmitted by Alice. $f_{\text{EC}}(E_\mu^{\text{OAM}})$ is the error correction efficiency of the signal state. $H_d(x) = -(1-x)\log_2(1-x) - x\log_2[x/(d-1)]$ is the d -dimensional Shannon entropy.

For decoy-state OAM-based QKD system, the transmittance η of single photon signal consists of the transmittance efficiency caused by misalignment and turbulence, as well as the internal loss at the receiver, which is expressed as:

$$\eta = \eta_{pe} \eta_{\text{atm}} \eta_{\text{Bob}} \eta_D \quad (21)$$

where η_{Bob} is the internal optical loss at Bob. η_D is the detection efficiency of SPD. Thus, Q_μ can be calculated by:

$$Q_\mu^{\text{OAM}} = Y_0 + 1 - e^{-\mu\eta} \quad (22)$$

where $Y_0 = 2p_d$ is the yield when Alice does not send a photon. p_d is the dark count of the detector. μ is the mean photon number of signal state. Meanwhile, considering the errors are induced by misalignment and crosstalk between states, E_μ^{OAM} can be given as [53]:

$$E_\mu^{\text{OAM}} = \frac{e_0 Y_0 + \varepsilon_t \times e_d (Q_\mu^{\text{OAM}} - Y_0)}{Q_\mu^{\text{OAM}}} \quad (23)$$

Different from the general two-dimensional QKD system, $e_0 = (d-1)/d$ is the error rate of the dark count in HD-QKD. Take into account the bit errors caused by misalignment and turbulence, $\varepsilon_t = 1 - P_{\text{at}} P_{pe}$ is the crosstalk probability.

By using ‘vacuum + weak decoy state’ method, the yield, the fraction and the error rate of the single-photon states Y_1^{OAM} , Δ_1 and e_1^{SUP} can be estimated by:

$$Y_1^{\text{OAM}} \geq Y_1^{L,v,0} = \frac{\mu}{\mu v - v^2} \left(Q_v^{\text{OAM}} e^v - Q_\mu^{\text{OAM}} e^\mu \frac{v^2}{\mu^2} - \frac{\mu^2 - v^2}{\mu^2} Y_0 \right) \quad (24)$$

$$\Delta_1 \geq \frac{\mu^2 e^{-\mu}}{\mu\nu - \nu^2} \left(\frac{Q_\nu^{\text{OAM}}}{Q_\mu^{\text{OAM}}} e^\nu - \frac{\nu^2}{\mu^2} e^\mu - \frac{\mu^2 - \nu^2}{\mu^2} \frac{Y_0}{Q_\mu^{\text{OAM}}} \right) \quad (25)$$

$$e_1^{\text{SUP}} \leq \frac{E_\nu^{\text{SUP}} Q_\nu^{\text{SUP}} e^\nu - e_0 Y_0}{Y_1^{L,\nu,0} \nu}. \quad (26)$$

3.2. Finite-key security analysis for decoy-state OAM-encoded HD-QKD

Due to the differences between HD-QKD and 2D-QKD in key analysis, the security of decoy-state OAM-encoded QKD has been obtained in the asymptotic regime, especially, in the limit of infinite-key effects. In the asymptotic case, the yield and the error rate of the single-photon state required by equation (19) can be estimated accurately from the measured values of OAM-encoded QKD, which will converge to the approximated true values. Then, the final key length of OAM-encoded QKD can be obtained safely. However, in the practical HD-QKD system, the number of quantum signal pulses emitted is limited, so there are statistical fluctuations between the observed and true values of the system parameters. When analyzing the security of HD-QKD system, it is necessary to consider the influence of finite-key effects response final security key rate caused by statistical fluctuation. Here, before giving a finite-key security analysis for OAM-encoded HD-QKD, we first review the improved Chernoff bound method used for fluctuation analysis in [65, 66]. For observation $\zeta > 0$, using the Chernoff inequality, the confidence interval for the expected value $E[\zeta]$ of the observed parameter can be obtained:

$$E^L[\zeta] = \frac{\zeta}{1 + \delta^L}, E^U[\zeta] = \frac{\zeta}{1 - \delta^U} \quad (27)$$

where $E^U[\zeta]$ and $E^L[\zeta]$ are the upper and lower limits of the confidence interval, δ^L and δ^U can be obtained from the following equations:

$$\left[\frac{e^{\delta^L}}{(1 + \delta^L)^{1 + \delta^L}} \right]^{\frac{\zeta}{1 + \delta^L}} = \frac{\varepsilon}{2}, \left[\frac{e^{-\delta^U}}{(1 - \delta^U)^{1 - \delta^U}} \right]^{\frac{\zeta}{1 - \delta^U}} = \frac{\varepsilon}{2} \quad (28)$$

where ε is the failure probability to estimate the confidence interval of the expected value.

Based on formulas (26) and (27), the upper and lower bounds of statistical fluctuation of overall gain and bit error rate of signal state and decoy state can be obtained. Furthermore, the upper and lower limits of the single-photon pulse overall gain and bit error rate are obtained by combining the formulas (23)–(25). Based on this, the security key length of OAM-basis of HD-QKD system under finite-key effects is obtained:

$$K^{\text{OAM},L} \geq M_{1\mu}^{\text{OAM},L} \left[1 - H_d \left(e_{1\mu}^{\text{SUP},U} \right) \right] - M_\mu^{\text{OAM}} f_{\text{EC}} \left(E_\mu^{\text{OAM},U} \right) H_d \left(E_\mu^{\text{OAM},U} \right) \quad (29)$$

where $M_{1\mu}^{\text{OAM},L}$ is the lower limit number of OAM-basis sifted key from the single-photon signal state. M_μ^{OAM} is the number of OAM-basis sifted key from the overall signal state. $e_{1\mu}^{\text{SUP},U}$ is the upper limit of the phase error rate. $E_\mu^{\text{OAM},U}$ is the upper limit of the QBER in the OAM-basis sifted key. Therefore, if the total number of quantum signal pulses emitted by Alice is N , then the final secret key rate of the practical HD-QKD system is:

$$R^L \geq \frac{K^{\text{OAM},L}}{N} \quad (30)$$

4. Numerical simulations

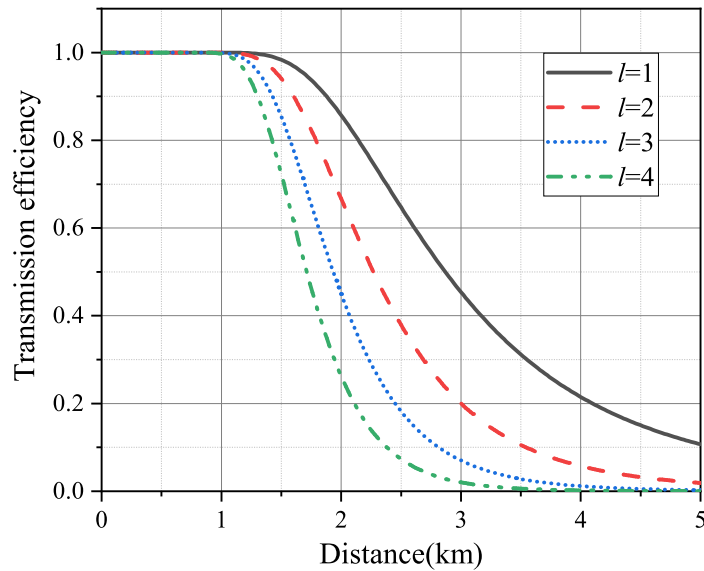
In view of the rotation invariance of the vortex light field, it effectively avoids the problem of the reference frame alignment, and provides a new coding scheme for the construction of high-speed and stable mobile quantum communication networks. The most likely application in the future is, for example, the scenario of drone-based quantum communication, with a typical distance range of kilometers. According to the above theoretical analysis, targeting 10 km free space link scenarios, the simulation method is used to analyze the influence of different factors on OAM-encoded HD-QKD system. The main parameters for simulation are as follows in table 1 [65, 67]:

4.1. Divergence of OAM beams propagation in free space

In order to evaluate the transmission characteristic of OAM under SDD, the relationship between distance and efficiency is shown in figure 5. As we mentioned above, different OAM states will suffer different amounts of diffraction, as do the OAM components of a SUP state. As shown in figure 5, for a long distance ($z \gg 1$ km), there are huge efficiency differences between lower-order and higher-order OAM states. This difference results in a nonuniform probability of detecting the OAM states, which deteriorates the system performance.

Table 1. Parameters used for the numerical simulation of OAM-encoded HD-QKD.

Parameters	Value
λ (wavelength)	1550 nm
w_0 (beam waist)	1 cm
C_n^2 (refractive-index structure parameter)	$1 \times 10^{-15} \text{ m}^{-2/3}$
D_r (receiving aperture)	260 mm
α (link attenuation coefficient)	$1.38 \times 10^{-4} (0.6 \text{ dB km}^{-1})$
Y_0 (background dark count rate)	3×10^{-6}
$f_{EC}(e_\mu)$ (error correction inefficiency)	1.15
e_d (misalignment error)	0.015
η_D (SPD efficiency)	0.5
η_{Bob} (internal transmittance of optical components)	0.9
ε (failure probability)	10^{-10}
N (finite size of data)	10^{13}
l (OAM index)	1, 2, 3, 4
D (transmission distance)	0–10 km

**Figure 5.** Transmission efficiency of OAM under SDD.

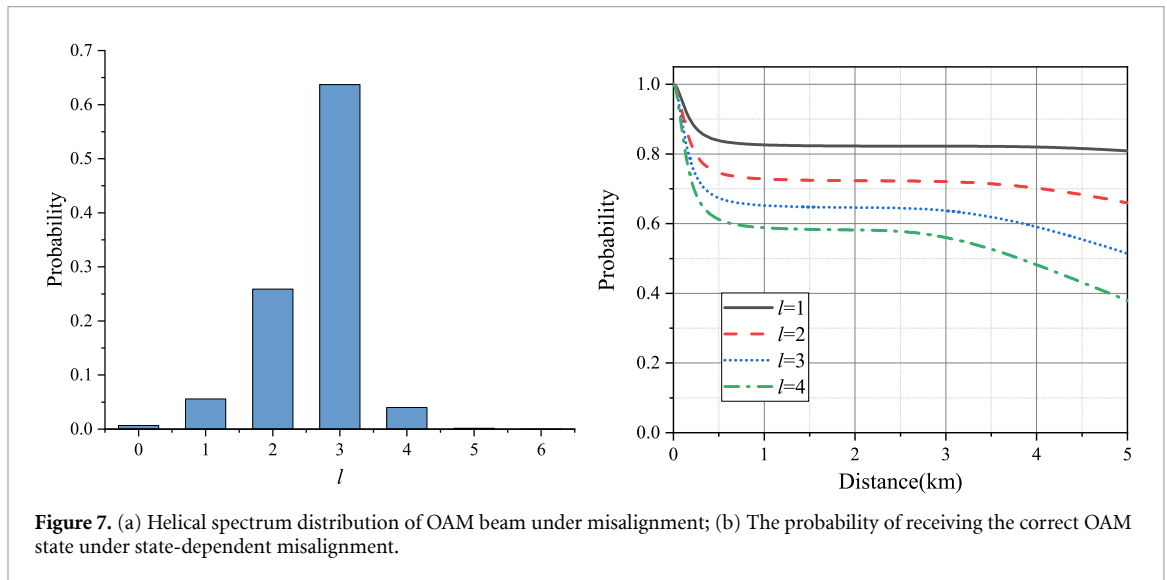
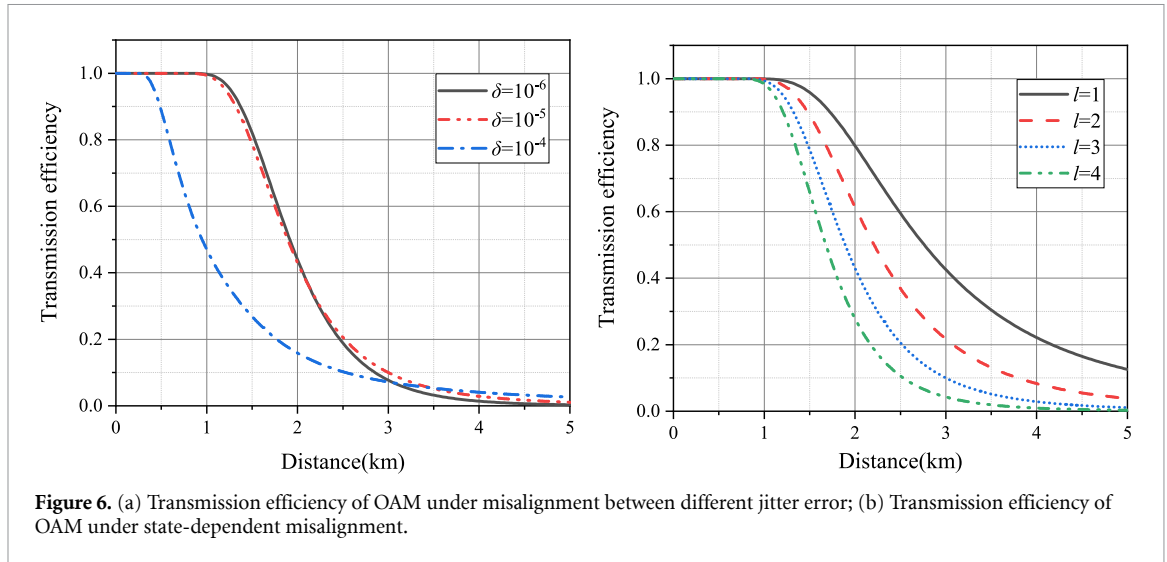
4.2. Misalignment of OAM beams propagation in free space

In view of the selection of jitter error at the transmitter, the variance of divergence angle is analyzed numerically. While holding w_0 of the LG mode constant, a convenient form for expressing the state-dependence of the beam divergence is given by [44]:

$$\alpha_l = \sqrt{\frac{|l|+1}{2}} \frac{2}{k_0 w_0}. \quad (31)$$

When $l = 4$, We get the beam divergence angle $\theta \approx 78.1 \mu \text{ rad}$. Therefore, the jitter error δ is determined according to this divergence angle, and the demand for APT system capability is evaluated. Three values of 10^{-6} , 10^{-5} and 10^{-4} were selected for simulation to analyze the signal transmission efficiency caused by misalignment under different variances. At the same time, similar to SDD analysis, the transmission efficiency of different OAM states under the misalignment is also analyzed.

As shown in the figure 6(a), a small angular jitter error has a greater advantage in short-distance transmission ($z \ll 3 \text{ km}$), which is higher for the transmission efficiency of the signal, and the impact of misalignment jitter in long-distance transmission can be negligible. Considering the cost of the system and the capability requirements for the APT system, $\delta = 10^{-5} \text{ rad}$ is selected as the angle jitter error for further analysis. Figure 6(b) demonstrates the state-dependent misalignment effect on transmission efficiency. The curve trend in figure 6(b) is similar to that in figure 5, indicating that misalignment has subtle impact on the state-dependent effects.



In order to test the influence of misalignment on the received error code, we select the helical spectrum distribution received at 3 km for analysis. Under the conditions of incident light OAM index $m = 3$ and radial index $p = 0$, the horizontal coordinate of figure 7(a) represents the OAM index l of each helical harmonic after the beam passes the misalignment, and the vertical coordinate represents the weight of the energy occupied by the helical harmonic component. The OAM index of incident light $m = 3$, the OAM components of the misaligned beam are mainly distributed in $l = 1, 2, 3, 4$. The OAM helical spectrum caused by the misalignment is not evenly distributed and focuses around $l = 3$. Lower-order OAM beam is easier to recognize and receive than higher-order OAM beam. Figure 7(b) shows that the probability of receiving helical spectrum distribution caused by misalignment is also affected by different OAM states. When the received OAM index is different from the incident light, it means that a bit error is received, which affects the performance of the system.

4.3. Turbulence of OAM beams propagation in free space

In order to demonstrate the transmission efficiency influenced by atmospheric turbulence and to provide data for SKR analysis, the transmission efficiency under strong ($C_n^2 = 10^{-13} \text{ m}^{-2/3}$), moderate ($C_n^2 = 10^{-14} \text{ m}^{-2/3}$) and weak ($C_n^2 = 10^{-15} \text{ m}^{-2/3}$) turbulence is simulated. As can be seen from figure 8, signal transmission can be effectively achieved under weak turbulence conditions.

The energy proportion of each helical harmonic component of incident light with OAM index after passing through 3 km atmospheric turbulence is shown in figure 9(a). The OAM components of the dispersing beam are mainly distributed in $l = 0, 1, 2, 3, 4, 5, 6$. Different from the misalignment, the incident OAM beam is diffused through the atmospheric turbulence, and the component of the beam is equal to the

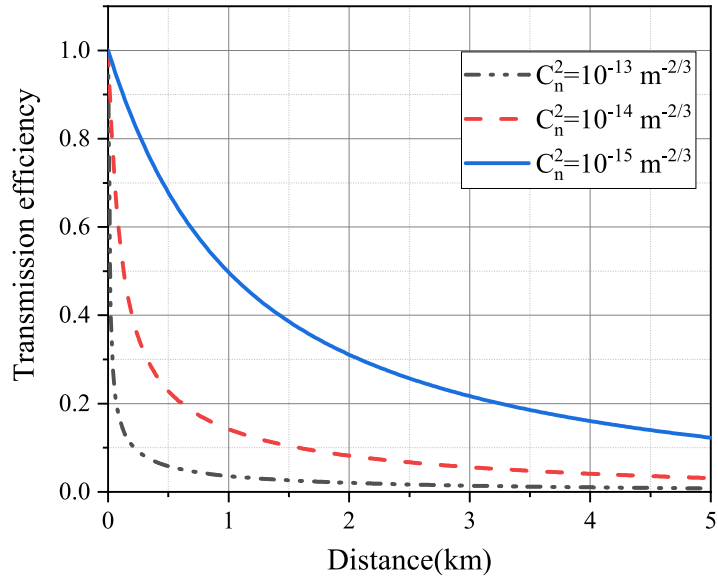


Figure 8. The transmission efficiency against the distance with different strength of atmospheric turbulence.

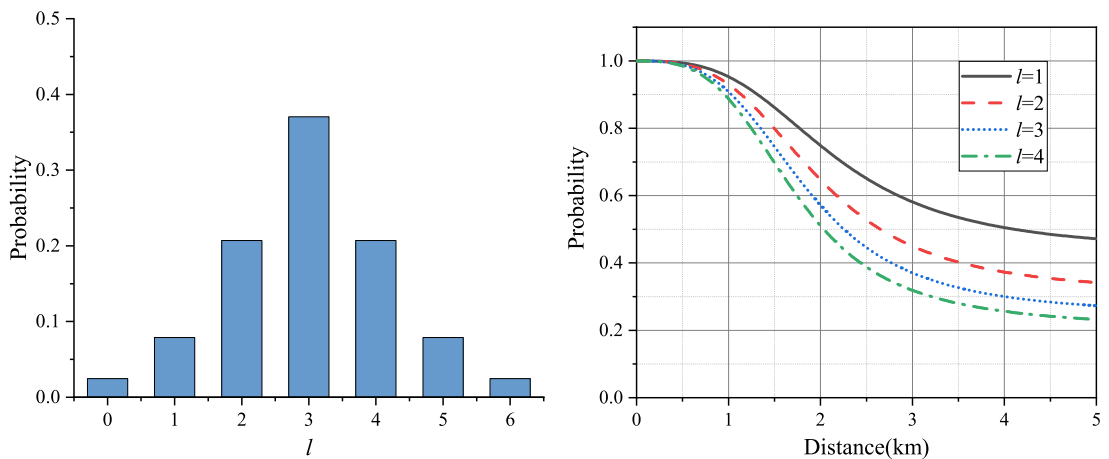


Figure 9. (a) Helical spectrum distribution of OAM beam under atmospheric turbulence; (b) the probability of receiving the correct OAM state under atmospheric turbulence between different OAM states.

original OAM, which means that the probability of receiving other states is symmetrical distribution centered on the receiving correct state. Figure 9(b) simulates the receiving probability of correct OAM states at different transmission distances, confirming the existence of state-dependent turbulence effect, and providing data support for subsequent high-dimensional QKD key analysis.

4.4. Performance of decoy-state OAM-encoded HD-QKD

In the above simulations, the theoretical model and simulation data of OAM transmission in atmospheric channel has been given. In order to further embody the application value of theoretical analysis, the performance of OAM encoded HD-QKD was evaluated. In practical HD-QKD, finite-key effects cannot be ignored. Therefore, we choose the finite size of data $N = 10^{13}$ to analyze the relationship between security key rate and transmission distance in different dimensions. It is worth noting that the QBER analysis of HD-QKD takes into account the effect of pointing error and atmospheric turbulence, and each OAM state sends and receives with equal probability.

As can be seen from figure 10, under the background of short-distance transmission, higher-dimensional QKD shows great advantages in the generation of SKR. In the context of long-distance transmission, 2D-QKD should be selected for key transmission, and 2D-QKD can transmit longer distances than higher-dimensional QKD. The above simulation results show that there is no direct relationship between the

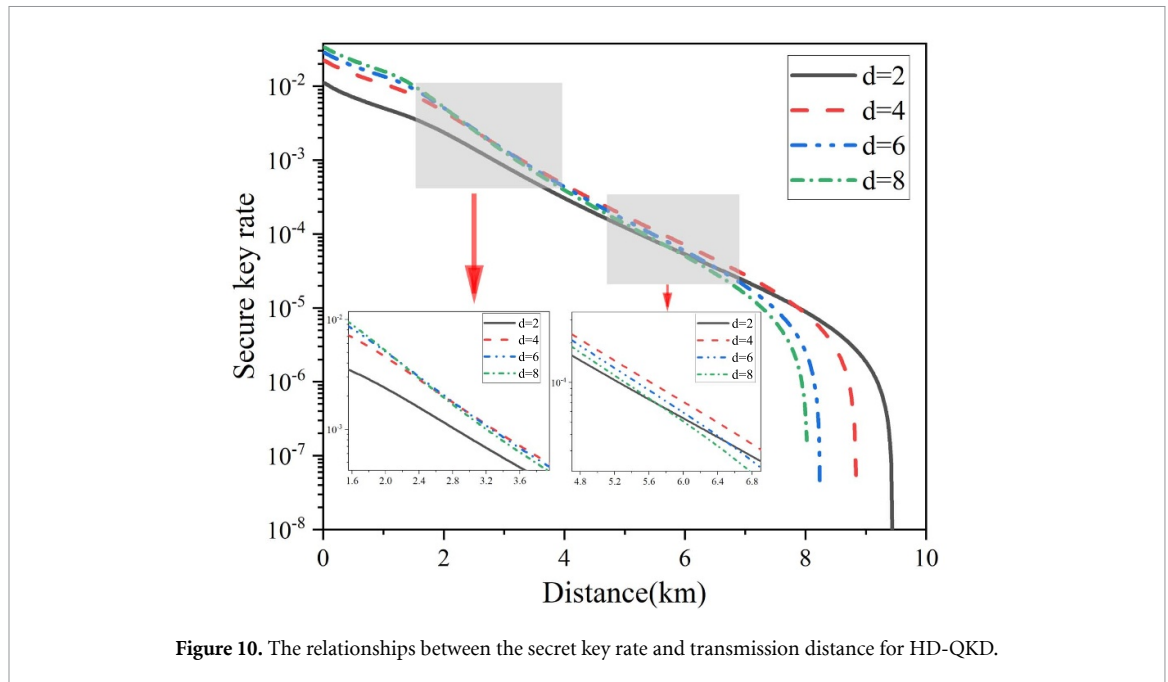


Figure 10. The relationships between the secret key rate and transmission distance for HD-QKD.

selection of QKD dimension and the performance of the system. In the actual scenario, we should choose the appropriate dimension according to the task requirements to implement QKD.

5. Discussion

OAM has been widely used in the field of quantum communication as a way of high-dimensional coding of optical field degrees of freedom. Although recent breakthrough experiments have demonstrated the feasibility of OAM-encoded HD-QKD, the underlying statistical characteristics of quantum atmospheric channels have not been well-understood and experimentally verified in the literature. The research in this paper enhances the theoretical completeness of HD-QKD. The main innovations of this study include the following aspects: (1) Aiming at the problem of SKR constraint caused by high-speed platform maneuvering in airborne scenarios, a complete OAM atmospheric transmission model is established, focusing on the analysis of state-dependent misalignment and turbulence effects, which are characterized by channel loss and mode crosstalk; (2) on the basis of atmospheric channel modeling, security analysis is performed on OAM-encoded HD-QKD, and quantitative evaluation of SKR and QBER is performed in combination with finite-key effects, thus providing theoretical reference for experiments.

This work holds significant reference value for future channel modeling studies. The OAM-encoded HD-QKD provides ideas for efficient information transfer of local hot spots between ground-air links, especially on airborne platforms. As the parameter settings here are temporary and ideal, and should be adjusted with the increase of distance, it is possible to develop a more comprehensive model. Consequently, the help of machine learning should have a better effect, which is the direction of our future research to facilitate the practical implementation of the system.

Data availability statement

All data that support the findings of this study are included within the article (and any supplementary files).

Acknowledgments

We gratefully thank Fumin Wang from Ministry of Education Key Laboratory for Nonequilibrium Synthesis and Modulation of Condensed Matter, Shaanxi Province Key Laboratory of Quantum Information and Quantum Optoelectronic Devices, School of Physics, Xi'an Jiaotong University for helpful discussions.

Ethics approval and consent to participate

Not applicable.

Conflict of interest

The authors declare that they have no competing interests.

Funding

This work is supported by the National Natural Science Foundation of China (Grant Nos. 61971436, 62073338).

ORCID iDs

Xingyu Wang  <https://orcid.org/0000-0002-1471-8668>

Yuexiang Cao  <https://orcid.org/0009-0004-9458-2124>

References

- [1] Gisin N, Ribordy G, Tittel W and Zbinden H 2002 Quantum cryptography *Rev. Mod. Phys.* **74** 145–95
- [2] Bennett C H and Brassard G 2014 Quantum cryptography: public key distribution and coin tossing *Theor. Comput. Sci.* **560** 7–11
- [3] Scarani V, Bechmann-Pasquinucci H, Cerf N J, Dušek M, Lütkenhaus N and Peev M 2009 The security of practical quantum key distribution *Rev. Mod. Phys.* **81** 1301–50
- [4] Zhou L, Lin J, Jing Y and Yuan Z 2023 Twin-field quantum key distribution without optical frequency dissemination *Nat. Commun.* **14** 928
- [5] Zhu H-T et al 2023 Experimental mode-pairing measurement-device-independent quantum key distribution without global phase locking *Phys. Rev. Lett.* **130** 030801
- [6] Liu Y et al 2023 Experimental twin-field quantum key distribution over 1000 km fiber distance *Phys. Rev. Lett.* **130** 210801
- [7] Li B et al 2022 Quantum state transfer over 1200 km assisted by prior distributed entanglement *Phys. Rev. Lett.* **128** 170501
- [8] Li Y et al 2022 Space-ground QKD network based on a compact payload and medium-inclination orbit *Optica* **9** 933–8
- [9] Chen Y-A et al 2021 An integrated space-to-ground quantum communication network over 4,600 kilometres *Nature* **589** 214–9
- [10] Popkin G 2021 The internet goes quantum *Science* **372** 1026–9
- [11] Bechmann-Pasquinucci H and Peres A 2000 Quantum cryptography with 3-state systems *Phys. Rev. Lett.* **85** 3313–6
- [12] Cerf N J, Bourennane M, Karlsson A and Gisin N 2002 Security of quantum key distribution using d -level systems *Phys. Rev. Lett.* **88** 127902
- [13] Mower J, Zhang Z, Desjardins P, Lee C, Shapiro J H and Englund D 2013 High-dimensional quantum key distribution using dispersive optics *Phys. Rev. A* **87** 062322
- [14] Wang F et al 2020 High-dimensional quantum key distribution based on mutually partially unbiased bases *Phys. Rev. A* **101** 032340
- [15] Otte E, Nape I, Rosales-Guzmán C, Denz C, Forbes A and Ndagano B 2020 High-dimensional cryptography with spatial modes of light: tutorial *J. Opt. Soc. Am. B* **37** A309–23
- [16] Gröblacher S, Jennewein T, Vaziri A, Weihs G and Zeilinger A 2006 Experimental quantum cryptography with qutrits *New J. Phys.* **8** 75
- [17] Etcheverry S, Cañas G, Gómez E S, Nogueira W A T, Saavedra C, Xavier G B and Lima G 2013 Quantum key distribution session with 16-dimensional photonic states *Sci. Rep.* **3** 2316
- [18] Zhong T et al 2015 Photon-efficient quantum key distribution using time-energy entanglement with high-dimensional encoding *New J. Phys.* **17** 022002
- [19] Mirhosseini M, Magaña-Loaiza O S, O’Sullivan M N, Rodenburg B, Malik M, Lavery M P J, Padgett M J, Gauthier D J and Boyd R W 2015 High-dimensional quantum cryptography with twisted light *New J. Phys.* **17** 033033
- [20] Krenn M, Handsteiner J, Fink M, Fickler R, Ursin R, Malik M and Zeilinger A 2016 Twisted light transmission over 143 km *Proc. Natl Acad. Sci.* **113** 13648–53
- [21] Cozzolino D, Da Lio B, Bacco D and Katsuo Oxenløwe L 2019 High-dimensional quantum communication: benefits, progress and future challenges *Adv. Quantum Technol.* **2** 1900038
- [22] Islam N T, Ci Wen Lim C, Cahall C, Kim J and Gauthier D J 2017 Provably secure and high-rate quantum key distribution with time-bin qudits *Sci. Adv.* **3** e1701491
- [23] Vagniluca I, Da Lio B, Rusca D, Cozzolino D, Ding Y, Zbinden H, Zavatta A, Oxenløwe L K and Bacco D 2020 Efficient time-bin encoding for practical high-dimensional quantum key distribution *Phys. Rev. Appl.* **14** 014051
- [24] Bulla L et al 2023 Nonlocal temporal interferometry for highly resilient free-space quantum communication *Phys. Rev. X* **13** 021001
- [25] Leach J, Bolduc E, Gauthier D J and Boyd R W 2012 Secure information capacity of photons entangled in many dimensions *Phys. Rev. A* **85** 060304
- [26] Boaron A et al 2018 Secure quantum key distribution over 421 km of optical fiber *Phys. Rev. Lett.* **121** 190502
- [27] Islam N T, Ci Wen Lim C, Cahall C, Qi B, Kim J and Gauthier D J 2019 Scalable high-rate, high-dimensional time-bin encoding quantum key distribution *Quantum Sci. Technol.* **4** 035008
- [28] Zahidy M et al 2024 Practical high-dimensional quantum key distribution protocol over deployed multicore fiber *Nat. Commun.* **15** 1651
- [29] Sit A et al 2017 High-dimensional intracity quantum cryptography with structured photons *Optica* **4** 1006–10
- [30] Wang F-X, Chen W, Yin Z-Q, Wang S, Guo G-C and Han Z-F 2019 Characterizing high-quality high-dimensional quantum key distribution by state mapping between different degrees of freedom *Phys. Rev. Appl.* **11** 024070
- [31] Molina-Terriza G, Torres J P and Torner L 2001 Management of the angular momentum of light: preparation of photons in multidimensional vector states of angular momentum *Phys. Rev. Lett.* **88** 013601
- [32] Cozzolino D et al 2019 Orbital angular momentum states enabling fiber-based high-dimensional quantum communication *Phys. Rev. Appl.* **11** 064058
- [33] Cañas G et al 2017 High-dimensional decoy-state quantum key distribution over multicore telecommunication fibers *Phys. Rev. A* **96** 022317

- [34] Sit A, Fickler R, Alsaïari F, Bouchard F'eric, Larocque H, Gregg P, Yan L, Boyd R W, Ramachandran S and Karimi E 2018 Quantum cryptography with structured photons through a vortex fiber *Opt. Lett.* **43** 4108–11
- [35] Gibson G, Courtial J, Padgett M J, Vasnetsov M, Pas'ko V, Barnett S M and Franke-Arnold S 2004 Free-space information transfer using light beams carrying orbital angular momentum *Opt. Express* **12** 5448–56
- [36] Chapman J C, Lim C C W and Kwiat P G 2022 Hyperentangled time-bin and polarization quantum key distribution *Phys. Rev. Appl.* **18** 044027
- [37] D'Ambrosio V, Nagali E, Walborn S P, Aolita L, Slussarenko S, Marrucci L and Sciarrino F 2012 Complete experimental toolbox for alignment-free quantum communication *Nat. Commun.* **3** 961
- [38] Zhang Y, Prabhakar S, Hamadou Ibrahim A, Roux F S, Forbes A and Konrad T 2016 Experimentally observed decay of high-dimensional entanglement through turbulence *Phys. Rev. A* **94** 032310
- [39] Wang Z, Malaney R and Burnett B 2020 Satellite-to-earth quantum key distribution via orbital angular momentum *Phys. Rev. Appl.* **14** 064031
- [40] Zhu L, Wang A, Deng M, Lu B and Guo X 2021 Free-space optical communication with quasi-ring airy vortex beam under limited-size receiving aperture and atmospheric turbulence *Opt. Express* **29** 32580–90
- [41] Willner A E et al 2021 Perspectives on advances in high-capacity, free-space communications using multiplexing of orbital-angular-momentum beams *APL Photon.* **6** 030901
- [42] Klug A, Peters C and Forbes A 2023 Robust structured light in atmospheric turbulence *Adv. Photon.* **5** 016006
- [43] Yi-Dong L, Chun-Qing G and Ming-Wei G 2008 Study on holographic grating diffraction for Laguerre-Gaussian beam generation *Chin. Phys. B* **17** 1769
- [44] Padgett M J, Miatto F M, Lavery M P J, Zeilinger A and Boyd R W 2015 Divergence of an orbital-angular-momentum-carrying beam upon propagation *New J. Phys.* **17** 023011
- [45] Sorelli G, Shatokhin V N, Roux F S and Buchleitner A 2018 Diffraction-induced entanglement loss of orbital-angular-momentum states *Phys. Rev. A* **97** 013849
- [46] Zhao J, Mirhosseini M, Braverman B, Zhou Y, Mohammad Hashemi Rafsanjani S, Ren Y, Steinhoff N K, Tyler G A, Willner A E and Boyd R W 2019 Performance analysis of d -dimensional quantum cryptography under state-dependent diffraction *Phys. Rev. A* **100** 032319
- [47] Ambuj A, Walla E, Andaloro S, Nomoto S, Vyas R and Singh S 2019 Symmetry in the diffraction of beams carrying orbital angular momentum *Phys. Rev. A* **99** 013846
- [48] Vasnetsov M V, Pas'ko V A and Soskin M S 2005 Analysis of orbital angular momentum of a misaligned optical beam *New J. Phys.* **7** 46
- [49] Li F, Jiang Y, Tang hua and Wang H 2009 Influences of misaligned optical beam carrying orbital angular momentum on the information transfer *Acta Phys. Sin.* **58** 6202
- [50] Wang H 2020 Performance of free space optical communication base on orbital angular momentum with pointing errors *IOP Conf. Ser.: Mater. Sci. Eng.* **711** 012080
- [51] Tyler G A and Boyd R W 2009 Influence of atmospheric turbulence on the propagation of quantum states of light carrying orbital angular momentum *Opt. Lett.* **34** 142–4
- [52] Wang X-Y, Zhao S-H, Dong C, Zhu Z-D and Gu W-Y 2019 Orbital angular momentum-encoded measurement device independent quantum key distribution under atmospheric turbulence *Quantum Inf. Process.* **18** 304
- [53] Wang X, Wu T, Dong C, Zhu H, Zhu Z and Zhao S 2021 Integrating deep learning to achieve phase compensation for free-space orbital-angular-momentum-encoded quantum key distribution under atmospheric turbulence *Photon. Res.* **9** B9–B17
- [54] Zhu Z, Janasik M, Fyffe A, Hay D, Zhou Y, Kantor B, Winder T, Boyd R W, Leuchs G and Shi Z 2021 Compensation-free high-dimensional free-space optical communication using turbulence-resilient vector beams *Nat. Commun.* **12** 1666
- [55] Chang Z, Wang Y, Guo Z, An M, Qu R, Jia J, Wang F and Zhang P 2023 Compact implementation of high-dimensional mutually partially unbiased bases protocol *Quantum Sci. Technol.* **8** 035028
- [56] Yin X, Chang H, Cui X, Ma J-X, Wang Y-J, Wu G-H, Zhang L and Xin X 2018 Adaptive turbulence compensation with a hybrid input-output algorithm in orbital angular momentum-based free-space optical communication *Appl. Opt.* **57** 7644–50
- [57] Zhao J, Zhou Y, Braverman B, Liu C, Pang K, Steinhoff N K, Tyler G A, Willner A E and Boyd R W 2020 Performance of real-time adaptive optics compensation in a turbulent channel with high-dimensional spatial-mode encoding *Opt. Express* **28** 15376–91
- [58] Tao Z, Ren Y, Abdulkirim A, Liu S and Rao R 2021 Mitigating the effect of atmospheric turbulence on orbital angular momentum-based quantum key distribution using real-time adaptive optics with phase unwrapping *Opt. Express* **29** 31078–98
- [59] Zhang H, Zheng W, Zheng G, Fu P, Qu J, Hoenders B J, Cai Y and Yuan Y 2021 Simultaneous measurement of orbital angular momentum spectra in a turbulent atmosphere without probe beam compensation *Opt. Express* **29** 30666–74
- [60] Liu J, Wang P, Zhang X, He Y, Zhou X, Ye H, Li Y, Xu S, Chen S and Fan D 2019 Deep learning based atmospheric turbulence compensation for orbital angular momentum beam distortion and communication *Opt. Express* **27** 16671–88
- [61] Wang K, Zhang M, Tang J, Wang L, Hu L, Wu X, Li W, Di J, Liu G and Zhao J 2021 Deep learning wavefront sensing and aberration correction in atmospheric turbulence *Photonix* **2** 1–11
- [62] Ghalaii M and Pirandola S 2023 Continuous-variable measurement-device-independent quantum key distribution in free-space channels *Phys. Rev. A* **108** 042621
- [63] Ma X, Qi B, Zhao Y and Lo H-K 2005 Practical decoy state for quantum key distribution *Phys. Rev. A* **72** 012326
- [64] Lo H-K, Ma X and Chen K 2005 Decoy state quantum key distribution *Phys. Rev. Lett.* **94** 230504
- [65] Zhao L-Y, Wu Q-J, Qiu H-K, Qian J-L and Han Z-F 2021 Practical security of wavelength-multiplexed decoy-state quantum key distribution *Phys. Rev. A* **103** 022429
- [66] Li J-H, Shi L, Li T-X, Xue Y, Zhang Z-Y and Tang J 2021 Parameters optimization based on neural network of practical wavelength division multiplexed decoy-state quantum key distribution *Mod. Phys. Lett. B* **35** 2150479
- [67] Wang L, Zhao S-M, Gong L-Y and Cheng W-W 2015 Free-space measurement-device-independent quantum-key-distribution protocol using decoy states with orbital angular momentum *Chin. Phys. B* **24** 120307